Food Chemistry 529 (2026) 151102

Contents lists available at ScienceDirect

Food Chemistry

journal homepage: www.elsevier.com/locate/foodchem

Decoding co-encapsulation of β-carotene and tocopherol in zein nanoparticles through orthogonal spectroscopy and machine learning

Roman M. Fortunatus [a], Diogo Cachetas [b,c], Sandor Balog [a,d], Laura Rodriguez-Lorenzo [b], Miguel Rocha [c,e], Dimitri Vanhecke [a,d], Barbara Rothen-Rutishauser [a], Patricia Taladriz-Blanco [a,*], Alke Petri-Fink [a,*]

[a] Adolphe Merkle Institute, University of Fribourg, 1700 Fribourg, Switzerland
[b] Water Quality Research Group, International Iberian Nanotechnology Laboratory, Av. Mestre José Veiga, Braga 4715-330, Portugal
[c] Center of Biological Engineering, University of Minho, Braga, Portugal
[d] National Center of Competence in Research Bio-Inspired Materials, University of Fribourg, Chemin des Verdiers 4, Fribourg 1700, Switzerland
[e] LABBELS - Associate Laboratory, Braga Guimarães, Portugal

ARTICLE INFO

Keywords:
Co-encapsulation
Non-covalent interactions
Raman spectroscopy
Chemometrics
Machine learning
Thermal stability
Correlative imaging

ABSTRACT

Protein-based nanoparticles (NPs), particularly zein NPs, are increasingly explored as oral carriers for nutrients and nutraceuticals due to their affordability, functionality, biodegradability, and biocompatibility. Co-encapsulation strategies can improve encapsulation efficiency and enhance the chemical stability of labile bioactive compounds; however, understanding the intermolecular interactions governing these systems remains challenging. In this study, zein NPs co-loaded with tocopherol (TC) and β-carotene (βC) at different ratios were investigated using Fourier Transform Infrared, fluorescence spectroscopy, and Raman hyperspectral imaging coupled with machine-learning analysis. TC incorporation enhanced both βC encapsulation efficiency and antioxidant activity. The 1:2 βC:TC ratio exhibited spectral signatures consistent with favorable intermolecular interactions, whereas a higher TC loading (1:3) showed spectral changes suggestive of perturbed non-covalent interactions. Raman spectral analysis further indicated that TC contributes to preserving βC stability under thermal conditions. These results advance understanding of co-encapsulation behavior and support the rational design of robust nanocarriers for labile nutraceutical compounds.

1. Introduction

Protein-based nanoparticles (NPs) offer promising platforms for nanoencapsulation and have recently attracted significant attention from food researchers due to their affordability, functionality, biodegradability, and biocompatibility (Fathi et al., 2018; Mohammadian et al., 2020; Ramos et al., 2022; Tarhini et al., 2017). Zein, a hydrophobic storage protein derived from corn (Shukla & Cheryan, 2001), has emerged as a versatile matrix for encapsulating labile bioactive molecules such as folate (Liu, Ma, et al., 2017), resveratrol (Huang et al., 2019), curcumin, (Tiwari et al., 2021) quercetin (Li et al., 2019), and beta-carotene (βC) (Chuacharoen & Sabliov, 2016; Mahalakshmi et al., 2020; Qiang et al., 2024). Zein NPs have been shown to improve the solubility of poorly water-soluble phytochemicals (Pan et al., 2014; Zhang, Li, et al., 2023), addressing a key limitation that hinders the broader utilization of these compounds. However, zein NPs often have limited colloidal stability in aqueous solutions near or above their isoelectric point, along with low encapsulation efficiency and chemical instability of the encapsulated compounds (Pascoli et al., 2018). Stabilizers, such as sodium caseinate, carrageenan, gum arabic (GA), and chitosan, have been employed to enhance colloidal stability, alongside physical treatments like high-pressure electrostatic treatments and cold plasma (He et al., 2025; Wang et al., 2024). Yet, these solutions do not fully resolve the limitations (Yuan et al., 2023).

An emerging strategy to preserve chemical stability and enhance bioactivity and functionality is co-encapsulation, where multiple bioactive compounds are incorporated within the same protein carrier (Cheng et al., 2023; Dissanayake & Bandara, 2024; Tadele et al., 2025). However, this approach introduces new complexity. Molecular interactions between the protein and the encapsulated cargo can significantly influence stability, conformation, and bioactivity of the cargo, thereby impacting encapsulation efficiency and release kinetics. While

* Corresponding authors.
E-mail addresses: patricia.taladrizblanco@unifr.ch (P. Taladriz-Blanco), alke.fink@unifr.ch (A. Petri-Fink).

https://doi.org/10.1016/j.foodchem.2026.151102
Received 8 December 2025; Received in revised form 30 May 2026; Accepted 7 September 2026
Available online 9 September 2026
0308-8146/© 2026 The Authors. Published by Elsevier Ltd. This is an open access article under the CC BY license (http://creativecommons.org/licenses/by/4.0/).

non-covalent interactions between protein side chains complexed with bioactive molecules have been widely studied using fluorescent (Joye et al., 2015; Wu et al., 2021), Fourier Transform Infrared (FTIR) spectroscopy (Lorenz-Fonfria, 2020) and their combination (Li et al., 2022; Lu et al., 2024; Nair, 2017; Zhang, Qi, et al., 2023; Zhao et al., 2022), investigations focusing on co-encapsulated systems in zein NPs remain limited (Dissanayake & Bandara, 2024). In particular, the use of Raman spectroscopy as an orthogonal analytical technique to complement fluorescence and FTIR approaches has been scarcely explored.

Compared to fluorescence or FTIR, Raman spectroscopy provides more detailed chemical information (Orlando et al., 2021) and supports quantitative analysis, with signal intensities correlating strongly with analyte concentrations (Chen et al., 2025; Portarena et al., 2023). Raman spectroscopy has been shown to detect conformational changes in disulfide bridges and the positioning of the tyrosine side chains in zein, even within complex food matrices (Sadat et al., 2022). Moreover, Raman spectra can resolve structural differences among βC isomers based on distinct peak positions and relative intensities of the C═C and C—C stretching bands (Novikov et al., 2021). Raman hyperspectral imaging further enables spatially resolved chemical analysis (Marin et al., 2024; Sun et al., 2024), although extracting meaningful information from high-dimensional data remains a challenge (Ren et al., 2025). Recent advances in machine learning and chemometric modeling (Pan et al., 2021; Zhou et al., 2025) have addressed this challenge, allowing accurate prediction of carotenoid composition and content across different fruit ripening stages (Kolašinac et al., 2021). Furthermore, differences in the Raman spectral features of carotenoids have been successfully exploited to distinguish α-carotene from β-carotene in carrots, based on their differing degrees of conjugation (Wang et al., 2021).

Although various nanocarrier systems, including lipid microparticles, Pickering emulsions, and protein-stabilized emulsions, have been extensively employed for the co-encapsulation of βC with other bioactive compounds such as curcumin, vitamin C, and quercetin, limited attention has been given to elucidating how mechanistic non-covalent interactions influence key functional properties, including chemical stability, encapsulation efficiency, and antioxidant activity (Brito-Oliveira et al., 2017; Dissanayake & Bandara, 2024; Wei et al., 2022; Xu et al., 2024). Only recently have data-driven Raman analyses, including PCA-based chemometrics, begun to identify interaction-sensitive vibrational signatures associated with encapsulation efficiency and intermolecular interactions in therapeutic delivery systems (Jin et al., 2026).

In this study, we investigated the molecular interactions underlying the co-encapsulation of βC, a vitamin A precursor (Grune et al., 2010) with antioxidant properties (Fryer, 1992), and α-tocopherol (TC) in zein NPs. TC was used as it has been reported to preserve the chemical stability of βC by scavenging degradative free radicals (Brito-Oliveira et al., 2017). To the best of our knowledge, this is the first study to integrate Raman hyperspectral imaging with machine-learning chemometric modeling to investigate zein-based co-encapsulation systems, complemented by orthogonal spectroscopic techniques. Key parameters included encapsulation efficiency, non-covalent interactions between components, and the thermal stability of encapsulated βC.

This orthogonal approach provides new insights into co-encapsulation dynamics and supports the rational design of stable zein-based nanocarriers for food applications.

2. Experimental section

2.1. Materials

Zein powder (88.0–96.35% protein) was obtained from Thermo Scientific, while gum Arabic (ACS reagent), ethanol (≥99.8% HPLC grade), beta carotene standard (≥95% HPLC grade), and alpha tocopherol (≥96% HPLC grade), 2, 20-Azino-bis (3-ethylbenzthiazoline-sulfonic acid) (ABTS, ≥98% HPLC grade), Trolox (≥96% HPLC grade), potassium persulfate (ACS reagent), 2,2-diphenyl-1-picrylhydrazyl (DPPH, Analytical grade) were obtained from Sigma Aldrich, while hexane (ACS reagent) was obtained from VWR Chemicals®. Ultrapure water (18.2 MΩ cm, 0.055 μS cm^{-1}) was produced in-house using a Sartorius Milli-Q system (Goettingen, Germany).

2.2. Synthesis of nanoparticles

Unloaded zein-based NPs were synthesized using the nano-precipitation method, following the protocol described by Zimath et al. (2023) with modifications. Specifically, 20 mg of zein powder was dissolved in 1 mL of 70% (v/v) ethanol and injected through a 21-gauge syringe into 20 mL of a 0.1% gum Arabic (GA) solution under magnetic stirring at 360 rpm. The mixture was continuously stirred at room temperature (RT) for 5 h to facilitate the evaporation of the organic solvent. The NPs were then collected by centrifuging 5 mL aliquots (repeated four times) for 12 min using an Amicon filter device with a molecular weight cutoff of 100 kDa at 1000×g. The particles were subsequently resuspended in water to achieve a final volume of 1 mL.

A similar procedure was employed to prepare loaded NPs, with a modification in the initial step involving the dissolution of zein powder. Specifically, an appropriate concentration of βC [400, 300, 200, 100, 50 μg/mL] and TC (both in acetone) was introduced into the organic phase (70% ethanol), ensuring that the total volume of the organic solution used for dissolving the zein powder remained consistent at 1 mL, as in the preparation of unloaded NPs.

An overview of the experimental methods and analytical approaches for each sample type is presented in Fig. S1.

2.3. Encapsulation efficiency (EE)

Extraction and determination of EE were carried out according to Mahalakshmi et al. (2020) with modifications. Briefly, 100 μL of the particles were destroyed by adding 300 μL of a 70% ethanol solution, followed by vortexing for 1 min. βC was extracted by adding 500 μL of hexane and gently mixing the solution using a Gyromini nutating agitator (Labnet International, Inc., NJ, USA) for 30 min. The sample was left undisturbed, and after 5 min, the hexane phase was carefully removed using a Pasteur pipette. This extraction process was repeated three times, and the collected aliquots were combined to achieve a final volume of 1.5 mL. The absorbance spectrum of the final solution was recorded using a Jasco UV–Vis spectrophotometer across a wavelength range of 200–800 nm. The concentration was quantified using a pre-established calibration curve (R^2 = 0.999) based on the maximum absorbance at 450 and 292 nm for βC and TC, respectively. EE was determined by the direct method, whereby EE was calculated as the ratio of the concentration of βC in disintegrated NPs to the initial βC concentration added during formulation (Sousa et al., 2017). The hexane extract was evaporated under a nitrogen stream at 35 °C, and the resulting residue was redissolved with 500 μL of acetone for HPLC analysis, following our previously established protocol (Fortunatus et al., 2025).

2.4. Antioxidant activities

The free radical scavenging capacity of βC/TC zein NPs was evaluated using $DPPH^{\bullet}$ and $ABTS^{\bullet+}$ assays according to Chen et al. (2023). DPPH activity was expressed as %DPPH activity calculated as the ratio of the absorbance difference between the control and sample to that of the control DPPH. ABTS scavenging activity was expressed as Trolox-equivalent antioxidant capacity (μM), and quantified using a Trolox calibration curve (0, 5, 10, 20, and 30 μM). To correct for background absorbance from the NP suspensions, the absorbance of a 20 μL NP dispersion (in 1 mL water) measured without ABTS was subtracted; this value was then subtracted from the control. The final ABTS

concentration was 58 μM in water.

2.5. Physicochemical characterization

The hydrodynamic diameter and zeta potential of the NPs were determined by dynamic light scattering (DLS) using an Anton Paar Litesizer 500 particle analyzer (Anton Paar, Graz, Austria) operating with a 658 nm laser, measuring the autocorrelation function at a scattering angle of 175°. Samples were appropriately diluted with Milli-Q water (pH = 6.0) before analysis. For thermal stability, 2 μL of NPs were added to 599 μL Milli-Q water and incubated at the appropriate temperatures for 15 min. After thermal treatment, samples were cooled to room temperature, further diluted with an additional 599 μL of Milli-Q water, and subsequently analyzed by DLS.

NPs were visualized by scanning electron microscopy (SEM) and Cryo-transmission electron microscopy (Cryo-TEM) using a Tescan Mira 3 SEM (Tescan, Brno, Czech Republic) and an FEI Tecnai Spirit TEM (ThermoFisher, Waltham, MA, USA), respectively.

For SEM, NPs were diluted in ultrapure water and drop-cast onto a silicon wafer mounted on an SEM stub with copper tape. After drying, the NPs were sputter-coated with 3.0 nm of gold using a Cressington Sputter Coater 208 HR (Cressington Scientific Instruments, Chalk Hill, UK) and observed at 2 kV.

For the Cryo-TEM, four microliters of the sample were drop-cast on a glow-discharged Lacey 400-carbon film grid (Agar Scientific, UK). The glow discharging was performed by ELMO Glow Discharge System (Cordouan Technologies, France) for 15 s, 2 mV at 2×10^{-1} bar. The sample was then blotted for 4 s in automatic blotting mode and then plunged into liquid ethane (−180 °C) using an EM GP2 Automatic Plunge Freezer (Leica Microsystems, Wetzlar, Germany). The cryo-plunger chamber was maintained at >90% humidity and 20 °C. Cryo-TEM images were acquired using an FEI Eagle CCD camera (ThermoFisher, Waltham, MA, USA) using the SerialEM acquisition software in low-dose mode (Mastronarde, 2005). Vitrification of the sample was checked by electron diffraction (data not shown). All additional image processing for SEM and TEM, including scale bar inclusion, contrast adjustments, blurriness improvement by a non-linear Mexican hat, and size distribution (automatic counting), was conducted using Fiji (ImageJ v1.53) (Schindelin et al., 2012).

Ultra-small-angle X-ray scattering (USAXS) measurements were conducted on the ID02 beamline at the European Synchrotron Facility (ESRF) in Grenoble, France. Zein NP suspended in water was filled into a rectangular glass (0.1, 1.0, and 0.07 mm, inner diameter, outer diameter, and wall thickness, respectively) capillary (VitroTubes, Tokyo, Japan) and then tightened with wax on both ends before USAXS measurement. The X-ray scattering spectrum was interpreted with a simple model assuming that the particles are homogeneous spherical objects. The corresponding form factor $P(q) = \frac{9\|(-qRCos[qR]+Sin[qR])\|^2}{q^6R^6}$ was obtained through a three-dimensional Fourier transform, and P(q) was expanded into a second-order polynomial around q = 0: $P(q) \cong b\left(1 - \frac{q^2R^2}{5}\right)$ where R is an average particle radius. This expression was regressed against the early points (Guinier regime) of the x-ray scattering spectra (Norbert, 2007).

2.6. Fluorescence spectroscopy

To explore the interaction mechanisms between zein NPs with βC and TC, fluorescence spectroscopy was carried out according to Zhang et al. (2022) in the liquid samples. For this, a Horiba Fluorolog 3 spectrometer with right-angle illumination equipped with a 450 W Xenon light source for excitation and an FL-1030-UP photomultiplier as detector was used to record the emission spectra at 290–500 nm with the excitation wavelength at 280 nm, respectively. The excitation and emission slits were set to 5 and 3 nm, respectively, all with an integration time of 0.1 s.

2.7. Fourier transform infrared spectroscopy and differential scanning calorimetry

Samples were dried at room temperature, and then about 2 mg of the sample was placed on an FTIR sample holder. Spectra were recorded using a PerkinElmer Spectrum 65 spectrometer with 10 scans per sample between 4000 and 500 cm^{-1} with a resolution of 1 cm^{-1}.

Differential Scanning Calorimetry (DSC) was performed to indirectly evaluate heat-associated physical and chemical transitions within the zein NPs, including changes in intermolecular interactions. (Peters et al., 2024) The phase transition temperatures of free or interfacial water within βC/TC zein NPs suspended in water were measured using a Mettler Toledo DSC 5+ STAR system under a nitrogen flow of 60 mL/min. Aliquots of 20 μL were placed into the DSC sample pans and hermetically sealed. Samples were subjected to three-heating/cooling cycles from −40 °C to 70 °C at a scanning rate of 10 °C/min.

2.8. Raman spectroscopy

All Raman measurements were performed using a WiTec Alpha 300 R confocal Raman microscope (WITec, Ulm, Germany) equipped with a 785 nm laser and an integrated CCD camera for acquiring bright-field images. The grating was set at 300 g/mm with a central wavelength of 899 nm, while the laser power was set at 50 mW. For the liquid samples, 100 μL of the sample was added to a 1 cm quartz cuvette, and then automated spectral maps were obtained from three areas within a randomly selected region. These maps were acquired in an area of 50 × 50 μm with 25 lines × 25 points per line using a 10× objective each for an integration time of 0.5 s, resulting in 1875 spectra.

For the thermal stability study, NPs were drop-cast on a silicon wafer (10 μL) and allowed to dry before thermal treatments. The dried samples were then placed in a preheated oven and sequentially heated at 25, 60, 80, 100, 120, 140, 160, and 180 °C for 15 min at each temperature. Raman measurements were acquired following each thermal treatment step. Raman maps were acquired in an area of 30 × 30 μm with 20 lines × 20 points per line, each for an integration time of 0.5 s using 50× objectives, resulting in 1200 spectra. The pre-processing of the obtained Raman spectra was carried out using the WITec Control 6 software, which included baseline correction by subtracting the measured background spectrum of each slide from the sample data, applying a shape subtraction filter of 100, and removing cosmic ray artefacts (Guo et al., 2021).

2.9. Molecular docking

Molecular docking simulations were conducted in this study using AutoDock Vina (v1.2.7) (Eberhardt et al., 2021; Trott & Olson, 2010) to investigate the non-covalent interactions between zein (receptor) and βC or TC (ligands). The zein structure (P06673) was obtained from the Swiss-model repository (https://swissmodel.expasy.org/) while the ligand structures for βC and TC were retrieved from the PubChem database. The initial protein structure was prepared in AutoDockTools (v1.5.7) by removing water molecules, adding polar hydrogen atoms, and assigning Kollman charges to generate a PDBQT file for docking. For βC and TC, Gasteiger–Hückel charges were assigned, nonpolar hydrogens were merged, and rotatable bonds were defined (Forli et al., 2016). A blind docking approach was employed by enclosing the entire protein within the grid box. Docking calculations were performed using the Vina algorithm with an exhaustiveness value of 50, the number of modes set to 10, and a grid spacing of 0.972 Å, while other parameters were maintained at default settings. The docking pose exhibiting the lowest binding free energy was considered the most favorable conformation and used for interaction analysis. The final binding modes between the ligands and zein were visualized using ChimeraX (v1.10.1).

2.10. Machine learning

The preprocessed spectra were cropped between 0 and 1800 cm^{-1} region prior to analysis. Two complementary feature-extraction strategies were evaluated: (i) full-spectrum analysis combined with dimensionality reduction methods to reduce redundancy and minimize overfitting; and (ii) extraction of peak-based spectral descriptors. For the peak-based approach, the following descriptors were extracted: height, prominence, width, width height, left minima, right minima, area under the curve (AUC) and peak position (Fig. S1) from specific peaks of interest, namely 310 cm^{-1}, 1008 cm^{-1}, 1156 cm^{-1} and 1516 cm^{-1}, using the find_peaks from scipy_signal version (1.15.2) with a tolerance window of ±10 cm^{-1} to account for peak shifts. An additional feature (peak ratio) was introduced to calculate the ratio between the height of 1516 cm^{-1} (βC C═C in-phase stretching) and 1156 cm^{-1} (βC C − C stretching) characteristic peaks, indicative of βC stability.

To assess the relevance of each feature extraction method, unsupervised ML methods such as Principal Component Analysis (PCA) and Uniform Manifold Approximation and Projection (UMAP) were applied, aiming to observe linear or non-linear patterns in a reduced-dimensional space that could facilitate visualization of sample clusters based on concentration.

For supervised learning, prediction of βC concentration was formulated as a regression task in which concentration values were treated as continuous numerical variables. The dataset was divided into training (80%) and test (20%) subsets using a stratified distance-based splitting strategy. Spectra were first grouped according to their corresponding concentration classes. For each concentration within each βC:TC ratio, a centroid was computed from the extracted spectral features, and the Euclidean distance between each spectrum and its corresponding class centroid was calculated using pairwise distances. Within each concentration group, spectra were ranked according to their distance from the centroid, with the spectra closest to the centroid assigned to the training subset (80%) and the most dissimilar spectra reserved for the test subset (20%).

This approach preserved the proportional representation of all concentration groups while providing a more conservative assessment of model generalization by evaluating the regression model on spectra exhibiting higher intraclass variability. An ExtraTreesRegressor model was selected due to its robust performance in handling high-dimensional spectral datasets and non-linear relationships. Model optimization and validation were performed using stratified 5-fold cross-validation on the training dataset, preserving the distribution of concentration groups across folds. Model performance was evaluated using the coefficient of determination (R^2), mean squared error (MSE), and mean absolute error (MAE). The final optimized model was subsequently evaluated on the independent test dataset using the same metrics.

In addition, to account for variability and spectral heterogeneity within each concentration group, an anomaly detection model (IsolationForest) was applied with a contamination parameter of 0.02. This conservative contamination value was selected to minimize the risk of misclassifying normal observations as anomalous while still enabling the detection of potential spectral outliers. The model assigned an anomaly score to each observation, classifying spectra with negative scores as outliers and spectra with positive scores as inliers (normal instances). The model was individually fitted to each sample concentration, and the anomaly score was displayed in the PCA embedding of each class.

2.11. Statistical analysis

One-way analysis of variance was applied to test the statistical difference in each dependent variable between different concentrations of encapsulated βC using R statistical software (R version 4.5.0 of 2025) (Team, 2025). The dependent variables were the emission wavelength at maximum fluorescent intensity, the maximum fluorescent intensity, and the Raman shift at maximum intensity. Treatments with p-value <0.05 were considered significant. Their Post-Hoc Analysis was performed with Tukey's Test using the agricolae package in R. Regarding machine learning and multivariate analysis, both supervised and unsupervised approaches were conducted in Python (Python Software Foundation, version 3.12.3 of 2024) for clustering, anomaly detection, and regression tasks.

3. Results and discussion

3.1. Synthesis, co-encapsulation, and non-covalent Interactions

βC-loaded zein NPs (Fig. 1a) were prepared by the nanoprecipitation method using gum arabic (GA), an ionic stabilizer. Spherical NPs with a narrow size distribution and a Feret diameter of 146 ± 54 nm ($n = 248$ NPs analyzed, Fig. S2a) were characterized using scanning electron microscope (Fig. S2b), dynamic light scattering (Fig. S2c), and cryogenic transmission electron microscopy (Fig. 1a). Other stabilizers, such as Pluronic F127, Tween 80, and polyvinyl alcohol (PVA) at 0.1% (m/v), were attempted. Still, the resulting NPs exhibited a broad size distribution for both unloaded (Fig. S2d-g) and βC-loaded NPs (Fig. S2h-i), and the zeta potential decreased as βC concentration increased (Fig. S2j).

Consistent with previous works (Andre de Almeida Campos et al., 2023; Wang et al., 2018), the sole encapsulation of βC within zein NPs yielded low encapsulation efficiency (EE) (Fig. 1b). To address the low EE when βC was encapsulated within zein NPs, βC and TC were co-encapsulated (hereinafter referred to as βC/TC zein NPs), aiming to leverage a synergistic effect to improve the EE of βC. TC was selected because it has been shown to enhance the stability of phytochemicals through a synergistic effect when encapsulated in zein NPs (Qiu et al., 2023; Tadele & Mekonnen, 2024; Zhang et al., 2019).

As hypothesized, and represented in Fig. 1b, a significantly higher EE (up to 56%) was observed for βC:TC ratios of 1:1 and 1:2 compared to ratios of 1:0 and 1:3, with the 1:0 ratio exhibiting the lowest EE (14%). DPPH and ABTS assays showed that incorporating TC increased antioxidant activity, with the βC:TC ratio of 1:0 exhibiting the lowest activity (Fig. 1c-d). In the DPPH assay, antioxidant activity increased progressively with TC concentration, with the βC:TC ratio of 1:3 exhibiting the highest radical scavenging activity across most βC concentrations, followed by the 1:2 formulation (Fig. 1c). In contrast, the ABTS assay showed maximal antioxidant activity for the 1:1 and 1:2 formulations, while the 1:3 formulation exhibited slightly lower values at higher βC concentrations (Fig. 1d). The differences observed between the DPPH and ABTS assays, particularly for the βC:TC 1:3 formulation, may be partially associated with differences in assay media and radical accessibility. Specifically, the ethanol–water medium used in the DPPH assay may promote partial dissolution of the zein NPs and facilitate the release of βC and TC, thereby enhancing radical scavenging activity. Similar differences between DPPH and ABTS responses in zein-based systems have also been reported in the literature (Liu, Pang, et al., 2017). A synergistic effect was also observed, as the EE and antioxidant activity of samples loaded with either βC or TC alone were generally lower than those of samples co-loaded with both βC and TC, especially for a 1:2 ratio (Fig. 1b-d).

Compared to previous studies, the EE of βC in this work was similar to that reported by Jain et al. (2018), but was slightly lower than that reported by Mahalakshmi et al. (2020). These differences likely reflect variations in processing methodology, as the present study employed a simple and scalable nanoprecipitation method, as reported by Jain et al., whereas Mahalakshmi et al. employed spray-drying. Notably, the EE achieved at the 1:2 βC:TC ratio was higher than that reported by Wang et al. (2018) for zein formulation prepared without tea polyphenols, although lower than for formulations containing such additives. Although the use of highly purified zein could potentially improve EE, such formulations may be less economically practical for large-scale food applications. Several approaches have been proposed to improve

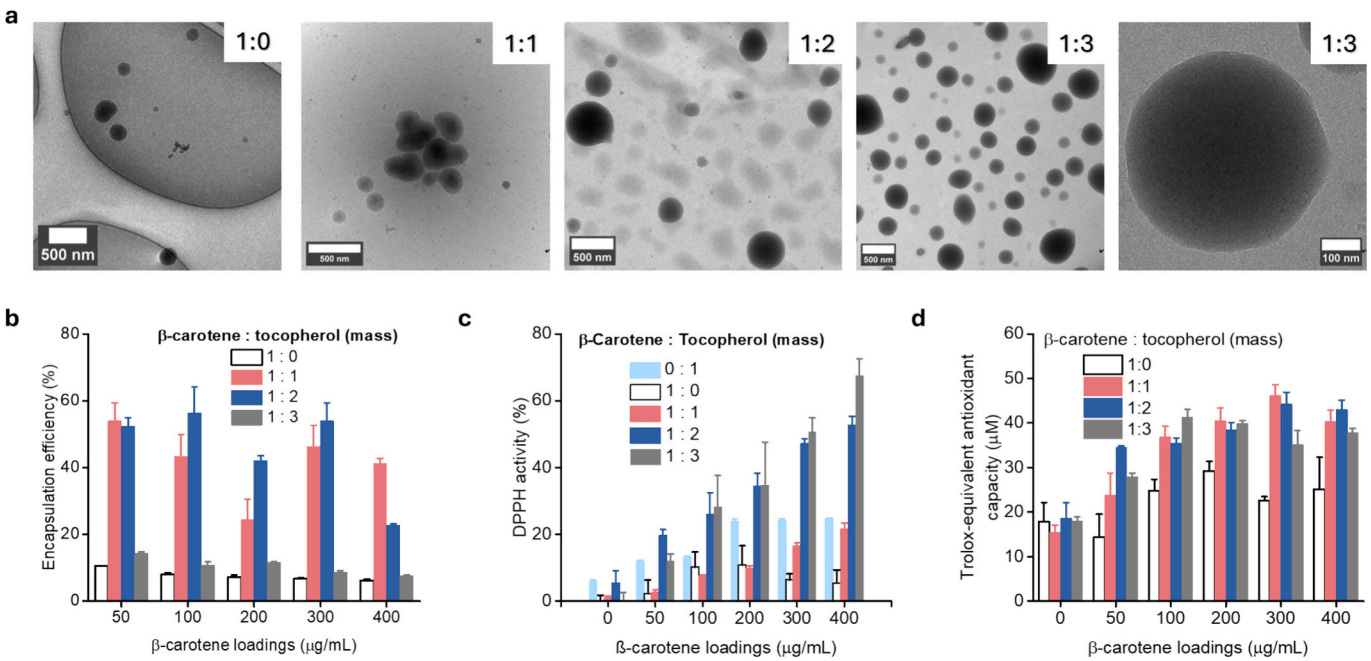


Fig. 1. Morphology, encapsulation efficiency, and antioxidant activity of βC:TC zein NPs. (a) Representative Cryo-TEM micrographs of zein NPs co-loaded with βC (300 μg/mL) and TC at different βC:TC ratios. The second micrograph for the 1:3 ratio is shown at higher magnification. (b) Encapsulation efficiency of βC determined by UV–Vis for the βC/TC zein NPs at βC:TC ratios of 1:0 (white), 1:1 (pink), 1:2 (blue), and 1:3 (grey). Antioxidant activity of βC:TC zein NPs across βC concentrations, measured by (c) DPPH assay and (d) ABTS assay, and expressed as Trolox Equivalent Antioxidant Capacity. Results are presented as triplicate analyses. (For interpretation of the references to color in this figure legend, the reader is referred to the web version of this article.)

the relatively low EE commonly associated with nanoprecipitated zein NPs. Among these, antisolvent *co*-precipitation has been shown to significantly enhance encapsulation performance through the formation of polymer–zein composite NPs, increasing EE from 36.34% to 93.56% (Lei & Lee, 2024). The concentration of TC associated (TC in the core as well as TC interacting with the particle surface) with the zein NPs was confirmed by HPLC (Fig. S3a), in which 50–60% of the added TC was directly associated with the particles. The higher βC EE observed in βC/TC zein NPs may also be attributed to the sacrificial oxidation of TC (Shibasaki-Kitakawa et al., 2011), which likely reduced the interaction of βC with free radicals or degradative amino acids present in the zein side chains (Hellwig, 2020).

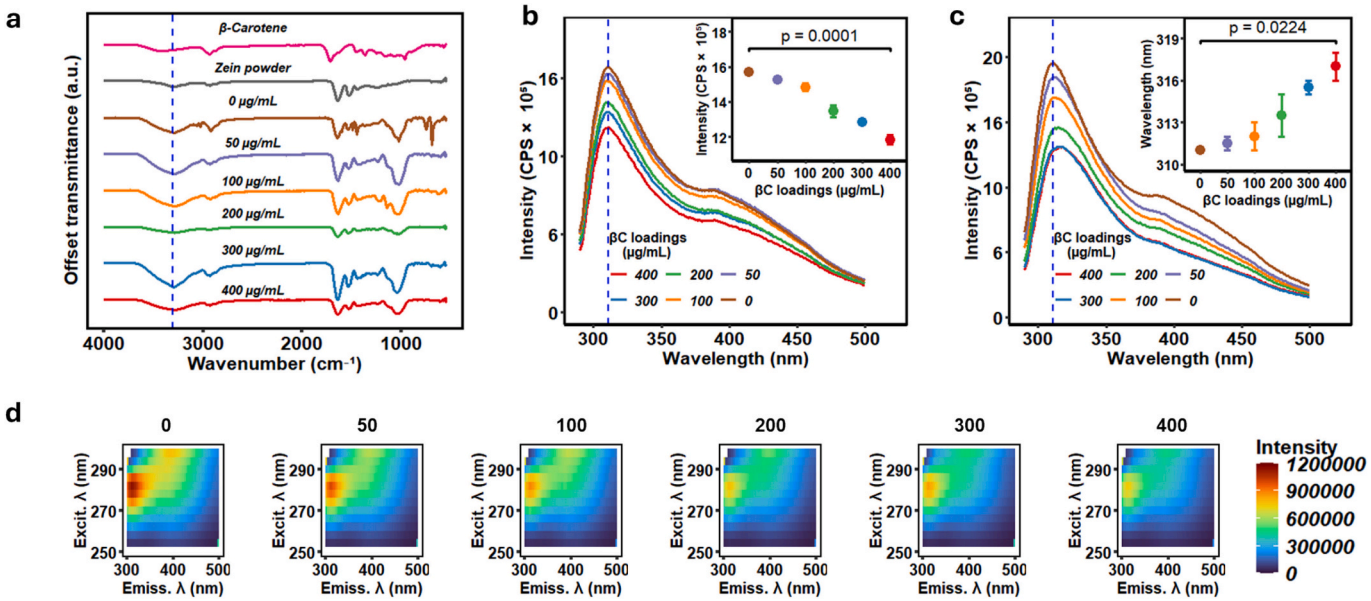


Fig. 2. Protein conformation changes on zein NPs co-loaded with βC:TC. (a) FTIR spectra of βC/TC zein NPs at the 1:0 ratio showing a shift in the –OH stretching band (dashed blue line) at 400 μg/mL βC, attributed to changes in hydrogen bonding. (b) Fluorescence spectra of βC/TC zein NPs at the 1:0 ratio, with increasing βC concentrations causing decreased fluorescence intensity, indicative of fluorescence quenching; this trend was observed for all βC:TC ratios (Table S1). (c) Fluorescence spectrum of βC/TC zein NPs at the 1:3 ratio showing a red shift in emission, indicating reduced hydrophobicity at higher TC content. Inserts in (b) and (c) show the maximum fluorescence intensity and corresponding wavelength, respectively. (d) False-color excitation–emission matrix plots of βC/TC zein NPs at the 1:0 ratio, highlighting spectral changes across the βC concentration range. Data are presented as mean ± standard error from duplicate analysis. (For interpretation of the references to color in this figure legend, the reader is referred to the web version of this article.)

βC/TC zein NPs were characterized by hydrodynamic diameter (Fig. S3b), zeta potential (Fig. 3c), and radius of gyration (Fig. 3d-h). As shown, the 1:1 and 1:2 ratios, which achieved the highest EE and reasonably high antioxidant activity, consistently maintained an average hydrodynamic diameter of ~300 nm across all βC concentrations (0–400 μg/mL). In contrast, the 1:0 and 1:3 ratios, associated with lower EE, exhibited an apparent decrease in hydrodynamic diameter as βC concentration increased, with the 1:3 ratio yielding the smallest NPs at every concentration tested. These trends were confirmed by USAXS (Fig. S3d–h), which demonstrated a consistent size reduction with increasing βC/TC ratios. Furthermore, NPs at a ratio of 1:0 displayed lower zeta potentials than their βC/TC counterparts across all conditions (Fig. S3c), highlighting distinct surface charge modifications upon TC incorporation.

To evaluate alterations in hydrogen bonding interactions, FTIR analysis (Fig. 2a) was first performed on the 1:0 βC/TC zein NPs, which showed the lowest EE. FTIR spectra revealed a shift in the zein band from 3293 cm^{-1} to 3286 cm^{-1} (assigned to –OH stretching, dashed blue line in Fig. 2a) at 400 μg/mL βC loading, while other zein fingerprint bands remained unchanged. In addition, the FTIR band positions corresponding to –OH, amide I (1641-1648 cm^{-1}), and amide II (1534–1540 cm^{-1}) stretching vibrations were compared across the studied ratios. These bands showed marked shifts in the 1:3 βC/TC zein NPs (Fig. S4a-d). Such spectral changes may reflect alterations in hydrogen-bonding interactions and suggest their involvement in the molecular organization of the system (Chen et al., 2026; Yu et al., 2020). At high βC concentrations, this may potentially compromise encapsulation performance.

DSC, which involves controlled temperature variation, can perturb zein structure through thermally induced denaturation and associated changes in intermolecular interactions such as hydrogen bonding (Hishida et al., 2023). The resulting thermal transition profiles, therefore, provide indirect information on protein–water interactions and may also indicate structural heterogeneity within zein NP systems (Sun et al., 2016). Consistent with this interpretation, the width of the DSC endothermic transition, attributed to the melting of confined or interfacial water, varied across the βC concentrations studied for the 1:0 and 1:3 βC/TC zein NPs (Fig. S4e-f), complementing the FTIR results discussed above.

Since βC is a hydrocarbon polyene, it interacts with zein mainly through hydrophobic forces (Fig. S5), as suggested by docking simulations showing βC incorporated into the hydrophobic cavities of zein moieties (Fig. S5a, yellow regions). On the other hand, TC is also a hydrophobic molecule; thus, co-loading βC and TC may lead to competition or saturation of zein's hydrophobic binding sites at higher concentrations, ultimately reducing the overall loading capacity. Additionally, TC has a single hydroxyl group capable of interacting with the asparagine or methionine side chains of zein through hydrogen bonding (Fig. S5c-d), and such interactions may disrupt the native hydrogen-bonding network that stabilizes the zein structure, thereby contributing to the reduced βC loading capacity. The binding energy and hydrogen bond distance between zein and TC predicted in this study (Fig. S5e) were in reasonable agreement with values previously reported in the literature (Liang & Zheng, 2023; Yakoubi, 2024). Although Vina is the best method in terms of docking power (Gaillard, 2018), it does not consider molecular flexibility, solvation effects, or dynamic behavior under physiological conditions (Kitchen et al., 2004).

To further evaluate hydrogen bonding and hydrophobic binding interactions, fluorescence measurements were performed. As shown in Fig. 2b, d, and Table S1, a general decrease in fluorescence intensity was observed with increasing βC concentration across most βC:TC ratios. This trend suggests fluorescence quenching potentially associated with increased molecular interactions, possibly due to βC/TC complexes interacting with tyrosine residues in the zein matrix (Wang & Fan, 2019). Zein proteins contain intrinsic fluorophores, including tyrosine, tryptophan, and phenylalanine, with emission properties sensitive to microenvironmental polarity (Lan et al., 2024; Tan et al., 2024; Zhu, Yao, et al., 2024). Phenylalanine, with a maximum excitation at 250 nm (Lu et al., 2024), exhibited negligible fluorescence intensity (Fig. S6a and S6c), consistent with its low quantum yield (Lakowicz, 2006). At 280 nm excitation, zein fluorescence predominantly originates from tyrosine, as zein contains minimal tryptophan (Li et al., 2022; Wu et al., 2021; Yu & Liang, 2022). GA also emits endogenous fluorescence (Sabet et al., 2021; Sethuraman & Rajendran, 2018, 2019). However, its contribution was negligible (Fig. S6b–c), since GA is a polysaccharide with a low fraction of protein (<3%) (Musa et al., 2018).

The interaction of βC/TC-tyrosine was explored using fluorescent quenching studies, whereby the quenching constants (k_q) exceeded the maximum dynamic diffusion quenching constant (10^{10} M^{-1} s^{-1}) in all samples (Table S2), consistent with a predominantly static quenching mechanism (Eftink & Ghiron, 1981). This suggests that the βC/TC molecules and tyrosine residues may form non-fluorescent ground-state complexes within the zein matrix. On the other hand, Stern–Volmer constants (Ksv) were not temperature-dependent for all ratios except 0:1 (Table S2 and Fig. S6e), suggesting that the co-encapsulated βC:TC interacts with zein through multiple types of noncovalent interactions, consistent with molecular simulation results. Such direct molecular interactions likely involve hydrophobic binding, hydrogen bonding, and/or Van der Waals forces, modifying the local microenvironment around the tyrosine residues (Lakowicz, 2006). In contrast, the 0:1 ratio showed decreases in K_{sv} and the apparent binding constant (K) with increasing temperature (Table S2 and Fig. S6e), indicating that TC interacts with zein predominantly through hydrogen bonding. Non-monotonic temperature-dependent trends across all βC-containing ratios suggest the coexistence of both static and dynamic fluorescence quenching mechanisms, consistent with the heterogeneous microenvironment of the zein NPs, with static quenching appearing to predominate (Yue et al., 2024).

Notably, beyond quenching effects, a red shift in maximum emission wavelength was detected with increasing βC concentrations for the 1:3 ratio (Fig. 2c, Fig. S6f, and Table S3), supporting the interpretation of changes in hydrophobicity in the local environment (Dos Santos Rodrigues et al., 2023; Zhu, Sun, et al., 2024) and/or protein conformational changes (Zhu, Yao, et al., 2024) driven by excess TC (Fig. S6g–h). These alterations in the protein matrix can contribute to changes in NP structural organization and encapsulation performance by disrupting protein–protein interactions, reducing network compactness (Zhang et al., 2021), and thereby diminishing the system's capacity to efficiently retain hydrophobic βC molecules, likely contributing to the compromised EE observed for the 1:3 ratio and its size reduction at βC concentrations above 100 μg/mL. In contrast, the maximum emission wavelength remained statistically unchanged across concentration in 1:2 βC:TC ratio, a finding consistent across three out of four temperatures (25 to 65 °C) studied (Table S3).

3.2. Chemometric analysis using Raman spectroscopy

Raman chemometric analysis can provide insight into relationships between molecular-level interactions and the practical performance (Guo et al., 2021)of βC-loaded zein NPs, supporting their rational design for real-world applications. Therefore, large-area Raman mapping (Yang et al., 2013) of βC/TC zein NPs samples in liquid, combined with both supervised and unsupervised machine learning (ML) algorithms (Pan et al., 2021) was employed to elucidate the interactions between βC, TC, and zein NPs. Liquid samples were measured since the Raman spectrum is highly spot-dependent (Butler et al., 2016; Zhou et al., 2025), especially for dried samples (Fig. S7a).

Using the full spectrum approach with dimensionality reduction with supervised regression methods resulted in a weak coefficient of regression ($R^2 = 0.28–0.76$) in all βC: TC ratios compared to the peaks feature extraction method ($R^2 > 0.996$) as shown in Table S4, as also suggested by the unsupervised embeddings of the Principal Component Analysis (PCA) and Uniform Manifold Approximation and Projection (UMAP).

Therefore, the feature extraction method based on interest peaks was selected for all liquid samples. Although relatively large numerical MSE values were obtained, these should be interpreted in the context of both the broad concentration range evaluated (0–400 μg/mL) and the squared-error formulation of the metric. In contrast, the MAE values remained consistently low across all βC:TC ratios (1.23–1.97 μg/mL), indicating minimal average prediction deviations relative to the experimental concentration range. The comparatively lower MSE and MAE values observed for the 1:2 and 1:3 ratios suggest greater spectral consistency and more robust concentration-dependent Raman features under higher TC contents.

As shown in Fig. 3a, the characteristic βC bands at 1516, 1156, and 1007 cm^{-1} corresponding to the C═C in-phase stretching (ν_1), C–C stretching (ν_2), and methyl in-plane rocking (ν_3) modes, respectively (Liu et al., 2007; Saito & Tasumi, 1983) were clearly identified in βC/TC zein NPs. These band intensities increased proportionally with βC concentration, ranging from 0 to 300 μg/mL. Notably, discrete carotenoid-associated Raman features were also detected in samples prepared without externally added βC (0 μg/mL condition), likely arising from endogenous carotenoid compounds naturally present in the commercial zein matrix derived from corn. Because these signals represent chemically relevant spectral contributions intrinsic to the material, they were retained during spectral preprocessing and not removed by baseline correction procedures. Importantly, the Raman-based chemometric analysis and machine learning models were primarily driven by concentration-dependent variations in spectral intensity, peak positions, band ratios, and overall multivariate spectral patterns, rather than solely by the presence or absence of carotenoid-associated bands.

Nevertheless, the presence of intrinsic carotenoid-like signals may reduce spectral specificity at low βC concentrations and should therefore be considered when interpreting the sensitivity limits of the Raman-based analysis. To further assess the influence of these endogenous carotenoid-associated bands, the relative background contribution of the 1516 and 1156 cm^{-1} Raman bands was quantified across all βC:TC formulations (Table S5). Residual Raman signals detected at 0 μg/mL βC represented approximately 10.9–27.0% and 13.3–22.9% of the maximum observed intensities for the 1516 and 1156 cm^{-1} bands, respectively.

Importantly, the relative contribution of the background signal progressively decreased with increasing βC concentration, particularly for the 1:1 and 1:2 formulations. Among the investigated ratios, the 1:2 ratio showed the lowest relative background interference for both carotenoid-associated bands, consistent with its lower intraclass variance in the LDA embeddings (Fig. 3f) and its improved regression performance.

Collectively, these results indicate that the supervised and unsupervised machine learning models were primarily governed by concentration-dependent spectral variations rather than by the intrinsic carotenoid-like background present in the zein matrix. Nonetheless, the endogenous Raman contribution may partially limit spectral specificity at low βC concentrations and should therefore be considered when interpreting the method's analytical sensitivity.

Quantitative spectral features (prominence, width, width at half-height, left and right minima, area under the curve, and peak position) extracted from the βC bands were initially analyzed using an unsupervised approach (Fig. 3b), suggested promising avenues for supervised tasks, since the data patterns display an ordered gradient in accordance with the different concentrations. These trends were further explored using supervised models, which successfully fitted a regression curve with excellent predictive performance regarding the concentration groups (R^2 values approaching unity; Fig. 3c).

Linear Discriminant Analysis (LDA) additionally confirmed the concentration gradient, with well-resolved clustering along the x-axis (Fig. 3d–g). Notably, LDA revealed that βC/TC zein NPs at a 1:2 ratio

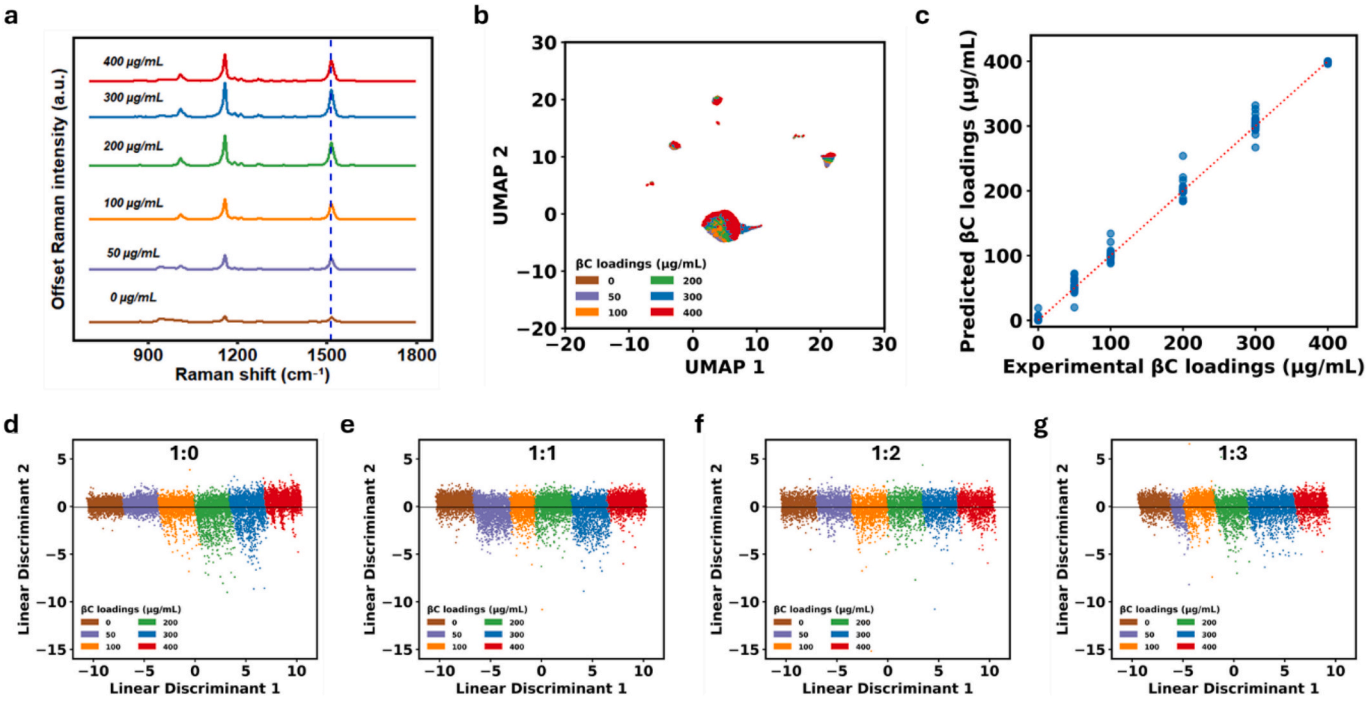


Fig. 3. βC:TC ratio-dependent interactions in zein NPs revealed by Raman spectroscopy and machine learning. (a) Representative Raman spectra of βC-loaded across increasing βC concentrations. Notably, carotenoid-associated bands are detected even at 0 μg/mL βC (1:0 ratio), indicating endogenous carotenoids in the zein matrix. (b) Unsupervised Uniform Manifold Approximation and Projection (UMAP) embedding – based on the features extracted from the peaks – demonstrates clusters with concentration gradients. (c) Supervised regression using an ExtraTrees regressor shows high predictive performance for βC concentration across all βC:TC ratios. (d-g) Linear Discriminant Analysis (LDA) embeddings reveal clear clustering along LD1 (x-axis) corresponding to βC concentration gradients. (f) At the 1:2 ratio and 300 μg/mL, LDA indicates notably low variance along LD2 (y-axis), reflecting enhanced intraclass spectral homogeneity compared to other ratios: (d) βC: TC 1:0, (e) βC: TC 1:1, and (g) βC: TC 1:3.

exhibited consistently low variance along Linear Discriminant 2 (LD2), indicating high intraclass spectral similarity, particularly at 300 μg/mL βC (Fig. 3f). In contrast, broader dispersion was observed for the 1:0, 1:1, and 1:3 ratios (Fig. 3d–g). The reduced interclass variance at 1:2, indicates greater spectral similarity among individual data points and suggests more homogeneous molecular environments across replicates, likely due to the slight amphiphilic character of TC (Martiel et al., 2014), which at 300 μg/mL βC, may promote stabilizing interactions, potentially contributing to βC stabilization within the protein network and reduced spectral heterogeneity. This uniformity is further supported by the highest encapsulation efficiency and strong antioxidant activity observed at this ratio (Fig. 1b-d), suggesting a favorable balance between cargo compatibility and matrix organization (Meinhardt-Wollweber et al., 2018). At lower TC contents (1:0), reduced stabilization may induce partial βC aggregation or uneven distribution, while at higher TC concentrations (1:3), excess TC may disrupt the protein network structure or induce phase separation (Figueiredo et al., 2025; Poudyal et al., 2023; Takma et al., 2023).

Building on the observed spectral uniformity at the 1:2 βC/TC ratio, we further examined the interactions between TC and βC within zein NPs across varying concentrations through an anomaly detection model, namely, an IsolationForest with a contamination parameter set to 0.02. As shown in Figs. 4a and S7b-d, the number of outliers progressively increased with rising βC concentration across all βC:TC ratios. This trend is accompanied by heightened sample variability, as evident from the PCA embedding.

Among the spectral features examined in both the ExtraTrees regressor and the IsolationForest models, shifts in the ν_1 (C═C stretching) mode of βC at 1516 cm^{-1} (highlighted by dotted lines in Fig. 3a), were selected to assess how TC modulates βC–zein interactions, given the high reactivity of this bond and its central role in βC oxidation (Havaux, 2014). As shown in Fig. 4b–e, a distinct redshift from ~1516 to 1513 cm^{-1} was observed with increasing βC/TC concentration consistent across all ratios except for the 1:2 ratio (Fig. 4d). Although a mechanistic study is required, the absence of a significant band shift at the 1:2 ratio across all concentrations is likely due to favorable molecular interactions among βC, TC, and zein, which may contribute to a more stable chemical environment for βC. This interpretation aligns with previous studies showing that a lower wavenumber at the ν_1 has been associated with α-carotene (Wang et al., 2021), suggesting that the spectral stability at the 1:2 ratio may reflect improved chemical stability of the encapsulated βC under these conditions. Moreover, the absence of Raman spectral shifts in βC encapsulated in electrospun zein fibers has been associated with retained chemical stability (Fernandez et al., 2009).

Despite extensive spectroscopic analysis, additional structural validation using high-resolution TEM and circular dichroism could further strengthen the interpretation of molecular organization among zein NPs with varying βC/TC ratios, representing an avenue for future studies.

3.3. Analysis of βC thermal stability

Initially, the 1:2 ratio, which exhibited the highest encapsulation efficiency, reasonably high antioxidant activity, and spectral features consistent with favorable molecular interactions among βC, TC, and zein, was selected for thermal degradation experiments. Thermal degradation experiments were conducted following an approach similar to that described by Knockaert et al. (2012); Medina-Gutiérrez et al. (2006) (Fig. 5), in which the 1:2 was directly compared with the free βC subjected to identical temperature-time conditions.

As shown in Fig. 5a–c, encapsulated βC demonstrated significantly lower degradation rates than free βC under thermal stress, demonstrated by the decreasing trend in intensity at 1516 cm^{-1} (ν_1, C═C in-phase stretching). This enhanced stability can be attributed to the protective shielding effect conferred by the zein NPs, which maintained their physical integrity even at elevated temperatures (Fig. S8a). The thermal stability of the NPs was further supported by the minimal changes observed in hydrodynamic diameter and polydispersity index for βC:TC zein NPs suspended in water and subjected sequentially to identical thermal conditions (Fig. S8d).

For both free and encapsulated βC systems, a slight increase in Raman intensity was observed between 25 °C and 80 °C (Fig. 4a–c), likely due to a reduction of residual free water remaining after room temperature drying, thereby increasing local sample concentration. To further examine zein's contribution to βC thermal stability, the ratio of the maximum intensity of the ν_1 (C═C, in-phase stretching) and ν_2 (C–C

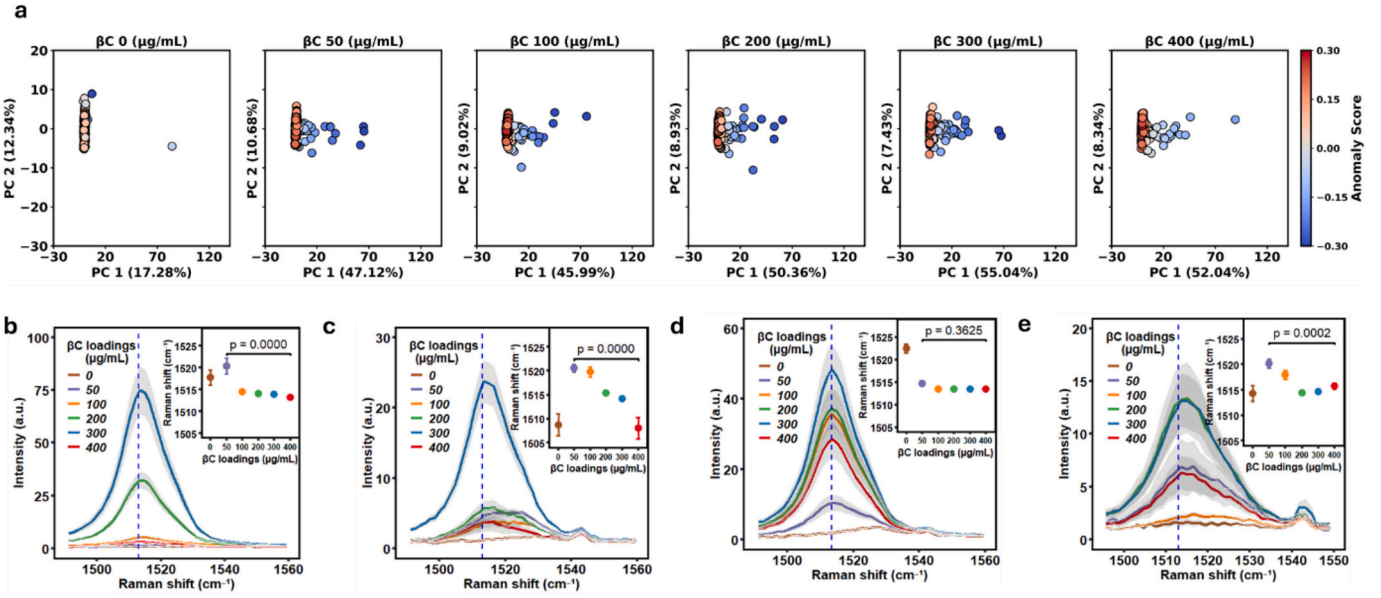


Fig. 4. Detailed Raman peak features evaluation approaches across C concentration for βC:TC ratio. (a) An anomaly plot generated using the IsolationForest outlier detection model applied to βC/TC zein NPs at a 1:2 ratio revealed an increase in the number of outliers, indicating greater spectral heterogeneity with rising βC concentrations, a trend also observed in other βC:TC ratios. (b-e) Average Raman spectra ($n = 50$) with the highest intensities for each formulation ratio: (b) 1:0, (c) 1:1, (d) 1:2, and (e) 1:3. The position and shift of the C═C stretching band at 1516 cm^{-1} were used to evaluate βC–zein interactions as a function of TC content and βC concentration.

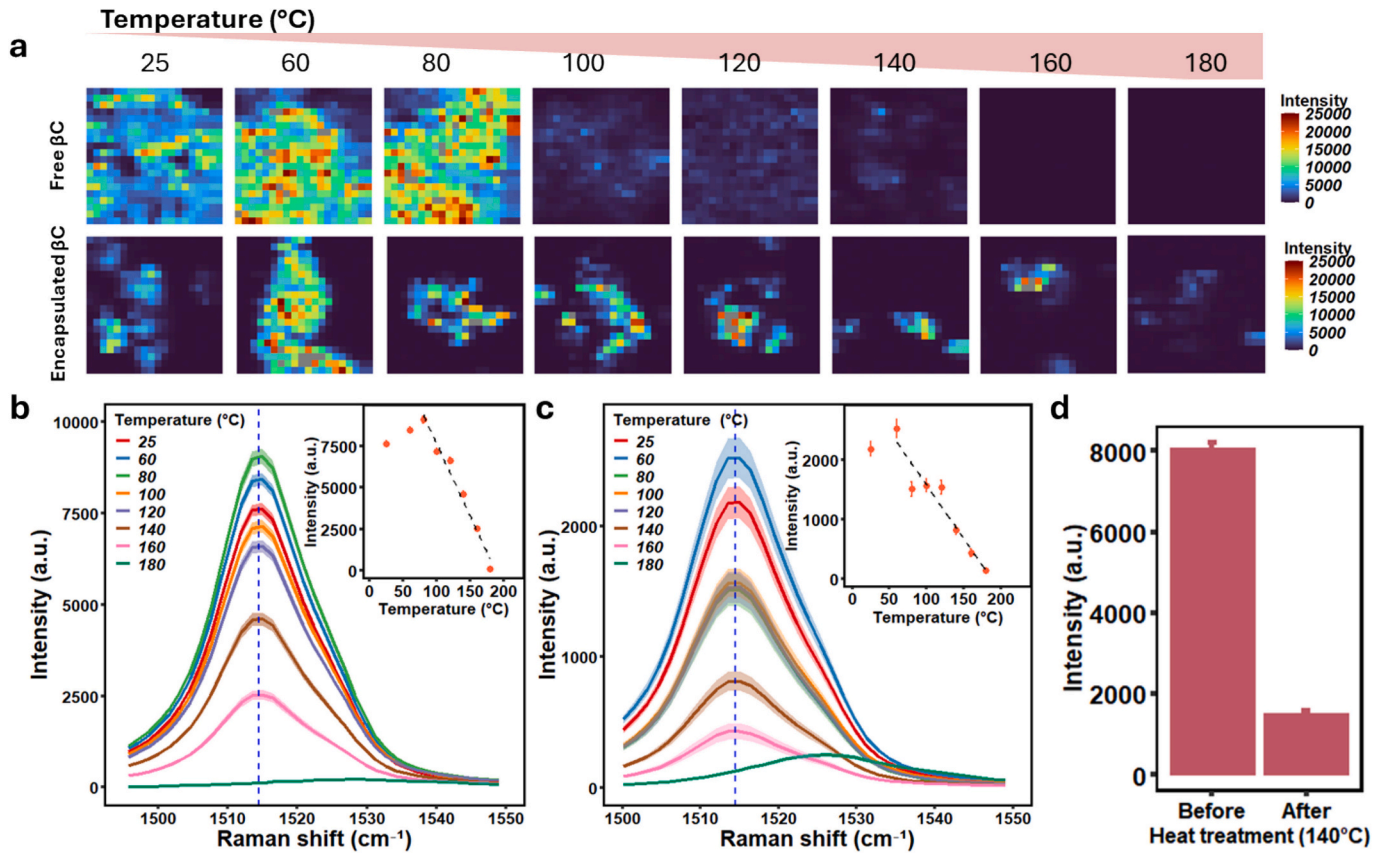


Fig. 5. Thermal stability of free and encapsulated βC evaluated by Raman spectroscopy. (a) Raman intensity of βC decreases with temperature, with a sharper decline observed for free βC compared to βC co-encapsulated with TC in zein NPs. False-color rendering is used for visualization; intensities reflect actual experimental values. (b-c) Temperature-dependent intensity changes of the ν_1 (C=C) Raman band for free βC and encapsulated βC:TC, respectively. Insets show linear fits of maximum intensity versus temperature, with slopes of −92 (free βC) and −15 (encapsulated βC), indicating improved thermal stability upon encapsulation. The dotted lines *on* the inserts represent the linear fit. A βC: TC sample containing 300 μg/mL of βC was used for both free and encapsulated conditions. (d) Average Raman intensity mapping before and after heating confirms spatially resolved spectral changes. Data represent the mean ± standard error from 1875 spectra. (For interpretation of the references to color in this figure legend, the reader is referred to the web version of this article.)

stretching) bands was determined as it relates to the stability of βC (Gong et al., 2020). The peak ratio decreased markedly with increasing temperature for free βC, indicating preferential degradation of C═C double bonds and, consequently, greater βC oxidation than the encapsulated form (Fig. S8e). Notably, the minimum ratios were achieved at 100 °C and 140 °C for free βC and encapsulated βC, consistent with a protective effect of zein encapsulation.

Thermal stability was subsequently compared across all βC:TC formulations. A similar temperature-dependent decrease in Raman intensity and red shift of the βC C═C stretching band was observed for encapsulated βC across βC/TC zein ratios (Fig. S8f–g). However, the magnitude of the red shift was slightly lower in the βC:TC zein NPs (1:1, 1:2, and 1:3) than in βC-loaded zein NPs (Fig. S8g). These results suggest that TC incorporation contributes may contribute to preserving βC chemical stability during thermal treatment across the investigated ratios. While the present study demonstrates the utility of Raman spectroscopy for monitoring βC thermal stability within zein NPs, the protective role of TC during heating has also been previously reported (Brito-Oliveira et al., 2017; Liu et al., 2015).

In addition, spatially resolved Raman mapping confirmed that intensity decreases with temperature by monitoring the same spot before and after thermal treatment (Fig. 5d and S8b–c). To validate the molecular origin of the measured signals, correlative scanning electron microscopy (SEM) coupled with Raman spectroscopy was conducted on the same location using a labeled grid, confirming that the Raman intensities corresponded to βC associated with zein NPs (Fig. S9a–c).

4. Conclusions and future directions

This study provides a comprehensive investigation of the molecular interactions and stability of zein NPs co-loaded with βC and TC using an orthogonal analytical strategy that combines FTIR, fluorescence spectroscopy, and Raman hyperspectral imaging integrated with machine learning.

Overall, TC incorporation enhanced both βC encapsulation efficiency and antioxidant activity, with the 1:1 and 1:2 βC:TC formulations exhibiting the most favorable balance of functional properties. In contrast, although the 1:3 formulation showed increased antioxidant activity in the DPPH assay, it was also associated with reduced encapsulation efficiency, suggesting perturbations in hydrogen-bonding and hydrophobic interactions within the zein matrix at higher TC loadings. The spectroscopic analyses indicated that TC modulates the molecular environment of βC within the zein matrix, potentially stabilizing the encapsulated compound through favorable non-covalent interactions. These effects were reflected by reduced fluorescence intensity, shifts in characteristic Raman bands, and enhanced thermal stability compared to free βC.

The Raman-based machine enabled detailed characterization of molecular interactions and stability trends, achieving high R^2 values in concentration prediction. At the 1:2 ratio, interclass variation was low, and no band shift was observed in the ν_1 mode (C=C) mode, consistent with improved βC stability. Furthermore, encapsulated βC at this ratio exhibited greater thermal stability compared to free βC (60–180 °C). Although the 1:2 βC:TC formulation showed enhanced stability

according to fluorescence and Raman analyses, TC incorporation generally contributed to preserving βC stability during thermal treatment across all investigated formulations.

These findings provide insight into co-encapsulation systems and support the rational design of stable, multifunctional nanocarriers for bioactive compounds. Further studies, including exposure of the system into simulated gastrointestinal conditions, in vitro digestion with food matrix, and bioaccessibility assessments, are warranted to evaluate the functional performance of these nanocarriers under physiologically relevant conditions.

Authors contribution

R. M. F. conceptualized and performed all the experiments included in this manuscript and analyzed the DLS, fluorescence, and HPLC data; was responsible for drafting the manuscript. D. C. developed, tested, and validated all ML models used in this manuscript. S. B. developed and tested the mathematical script to analyze the USAXS data from the synchrotron and was responsible for DLS data interpretation. L. R. L. and M. R. supervised D. C. and assisted in the conceptualization and interpretation of ML outputs. D. V. assisted with the Cryo-TEM sample preparation and imaging. B. R. R. provided resources, supervised, and edited the manuscript. P. T. B. was responsible for study conceptualization, data interpretation, supervision, and manuscript drafting. A. P. F. contributed to the conceptual development of the study through regular discussions and provided input throughout the project. She also revised and edited the manuscript. All authors have approved the final version of the manuscript.

CRediT authorship contribution statement

Roman M. Fortunatus: Writing – review & editing, Writing – original draft, Visualization, Software, Methodology, Investigation, Data curation, Conceptualization. **Diogo Cachetas:** Writing – review & editing, Visualization, Software, Formal analysis. **Sandor Balog:** Writing – review & editing, Validation, Software, Formal analysis. **Laura Rodriguez-Lorenzo:** Writing – review & editing, Validation, Supervision, Formal analysis. **Miguel Rocha:** Writing – review & editing, Validation, Supervision, Software. **Dimitri Vanhecke:** Writing – review & editing, Visualization, Validation, Formal analysis. **Barbara Rothen-Rutishauser:** Writing – review & editing, Supervision, Project administration, Funding acquisition. **Patricia Taladriz-Blanco:** Writing – review & editing, Writing – original draft, Validation, Methodology, Formal analysis, Conceptualization. **Alke Petri-Fink:** Writing – review & editing, Supervision, Resources, Project administration, Funding acquisition, Conceptualization.

Declaration of competing interest

The authors declare that they have no known competing financial interests or personal relationships that could have appeared to influence the work reported in this paper.

Acknowledgements

The authors acknowledge support from the Swiss Excellence Scholarship through the State Secretariat for Education, Research and Innovation (ESKAS 2022.508) and the Adolphe Merkle Foundation. The authors also acknowledge the European Synchrotron Radiation Facility (ESRF), Grenoble, France, for granting beamtime on beamline ID02 through the proposal SC-5454. The authors would like to thank Dr. Gouranga Manna for his assistance during the USAXS data acquisition. L. R.-L. acknowledges funding from FCT for the Scientific Employment Stimulus Program (2020.04021.CEECIND). D.C. acknowledges FCT for the Ph.D. scholarship 2024.01218.BDANA.

Appendix A. Supplementary data

Supplementary data to this article can be found online at https://doi.org/10.1016/j.foodchem.2026.151102.

Data availability

The data supporting this article have been included as part of the supplementary information. Raw data can be accessed on Zenodo via https://zenodo.org/records/16811359

References

Andre de Almeida Campos, L., Francisco Silva Neto, A., Cecilia Souza Noronha, M., Ferreira de Lima, M., Macario Ferro Cavalcanti, I., & Stela Santos-Magalhaes, N. (2023). Zein nanoparticles for drug delivery: Preparation methods and biological applications. *International Journal of Pharmaceutics, 635*, Article 122754. https://doi.org/10.1016/j.ijpharm.2023.122754

Brito-Oliveira, T. C., Molina, C. V., Netto, F. M., & Pinho, S. C. (2017). Encapsulation of Beta-carotene in lipid microparticles stabilized with hydrolyzed soy protein isolate: Production parameters, alpha-tocopherol coencapsulation and stability under stress conditions. *Journal of Food Science, 82*(3), 659–669. https://doi.org/10.1111/1750-3841.13642

Butler, H. J., Ashton, L., Bird, B., Cinque, G., Curtis, K., Dorney, J., … Martin, F. L. (2016). Using Raman spectroscopy to characterize biological materials. *Nature Protocols, 11*(4), 664–687. https://doi.org/10.1038/nprot.2016.036

Chen, H., Lin, S., Wu, J., Xu, Y., Cai, X., & Wang, S. (2023). The structure, antioxidant activity, and stability of fish gelatin/chitooligosaccharide nanoparticles loaded with apple polyphenols. *Journal of the Science of Food and Agriculture, 103*(8), 4211–4220. https://doi.org/10.1002/jsfa.12455

Chen, S., Jia, J., Du, J., Qin, N., & Xia, X. (2026). Fabrication of a zein-phloretin complex and nanoparticles: Interaction mechanism and characterization. *RSC Advances, 16*(9), 7717–7725. https://doi.org/10.1039/d5ra08898d

Chen, Y., Yang, Z., Zeng, S., Tian, H., Cheng, Q., Lv, S., & Li, H. (2025). Quantitative analysis of beta-carotene and unsaturated fatty acids in blended olive oil via Raman spectroscopy combined with model prediction. *Food Chemistry, 470*, Article 142621. https://doi.org/10.1016/j.foodchem.2024.142621

Cheng, H., Chen, W., Jiang, J., Khan, M. A., Wusigale, & Liang, L. (2023). A comprehensive review of protein-based carriers with simple structures for the co-encapsulation of bioactive agents. *Comprehensive Reviews in Food Science and Food Safety, 22*(3), 2017–2042. https://doi.org/10.1111/1541-4337.13139

Chuacharoen, T., & Sabliov, C. M. (2016). The potential of zein nanoparticles to protect entrapped β-carotene in the presence of milk under simulated gastrointestinal (GI) conditions. *LWT - Food Science and Technology, 72*, 302–309. https://doi.org/10.1016/j.lwt.2016.05.006

Dissanayake, T., & Bandara, N. (2024). Protein-based encapsulation systems for codelivery of bioactive compounds: Recent studies and potential applications. *Current Opinion in Food Science, 57*. https://doi.org/10.1016/j.cofs.2024.101181

Dos Santos Rodrigues, F. H., Delgado, G. G., Santana da Costa, T., & Tasic, L. (2023). Applications of fluorescence spectroscopy in protein conformational changes and intermolecular contacts. *BBA Advances, 3*, Article 100091. https://doi.org/10.1016/j.bbadva.2023.100091

Eberhardt, J., Santos-Martins, D., Tillack, A. F., & Forli, S. (2021). AutoDock Vina 1.2.0: New docking methods, expanded force field, and Python bindings. *Journal of Chemical Information and Modeling, 61*(8), 3891–3898. https://doi.org/10.1021/acs.jcim.1c00203

Eftink, M. R., & Ghiron, C. A. (1981). Fluorescence quenching studies with proteins. *Analytical Biochemistry, 114*(2), 199–227. https://doi.org/10.1016/0003-2697(81)90474-7

Fathi, M., Donsi, F., & McClements, D. J. (2018). Protein-based delivery systems for the nanoencapsulation of food ingredients. *Comprehensive Reviews in Food Science and Food Safety, 17*(4), 920–936. https://doi.org/10.1111/1541-4337.12360

Fernandez, A., Torres-Giner, S., & Lagaron, J. M. (2009). Novel route to stabilization of bioactive antioxidants by encapsulation in electrospun fibers of zein prolamine. *Food Hydrocolloids, 23*(5), 1427–1432. https://doi.org/10.1016/j.foodhyd.2008.10.011

Figueiredo, M., Sarkany, Z., Rocha, F., & Martins, P. M. (2025). Challenges and advances in the encapsulation of bioactive ingredients using whey proteins. *Foods, 14*(4). https://doi.org/10.3390/foods14040691

Forli, S., Huey, R., Pique, M. E., Sanner, M. F., Goodsell, D. S., & Olson, A. J. (2016). Computational protein-ligand docking and virtual drug screening with the AutoDock suite. *Nature Protocols, 11*(5), 905–919. https://doi.org/10.1038/nprot.2016.051

Fortunatus, R. M., Balog, S., Sousa, F., Vanhecke, D., Rothen-Rutishauser, B., Taladriz-Blanco, P., & Petri-Fink, A. (2025). Taylor dispersion analysis and release studies of beta-carotene-loaded PLGA nanoparticles and liposomes in simulated gastrointestinal fluids. *RSC Advances, 15*(2), 1095–1104. https://doi.org/10.1039/d4ra08138b

Fryer, M. J. (1992). The antioxidant effects of thylakoid vitamin E (α-tocopherol). *Plant, Cell & Environment, 15*(4), 381–392. https://doi.org/10.1111/j.1365-3040.1992.tb00988.x

Gaillard, T. (2018). Evaluation of AutoDock and AutoDock Vina on the CASF-2013 benchmark. *Journal of Chemical Information and Modeling, 58*(8), 1697–1706. https://doi.org/10.1021/acs.jcim.8b00312

Gong, N., Yao, F., Wang, J., Fang, W., Sun, C., & Men, Z. (2020). Excited state geometry of beta-carotene influenced by environments: The nature and decisive role of solvent revealing by two-dimensional resonance Raman correlation spectroscopy. *Optics Express, 28*(22), 33068–33076. https://doi.org/10.1364/OE.404647

Grune, T., Lietz, G., Palou, A., Ross, A. C., Stahl, W., Tang, G., … Biesalski, H. K. (2010). Beta-carotene is an important vitamin A source for humans. *The Journal of Nutrition, 140*(12), 2268S–2285S. https://doi.org/10.3945/jn.109.119024

Guo, S., Popp, J., & Bocklitz, T. (2021). Chemometric analysis in Raman spectroscopy from experimental design to machine learning-based modeling. *Nature Protocols, 16*(12), 5426–5459. https://doi.org/10.1038/s41596-021-00620-3

Havaux, M. (2014). Carotenoid oxidation products as stress signals in plants. *The Plant Journal, 79*(4), 597–606. https://doi.org/10.1111/tpj.12386

He, W., Bian, Y., Guo, K., Chen, Y., Chen, G., & Li, S. (2025). Electric field-induced enhances the stability and bioactivity of zein-based nutrient delivery systems. *Food Hydrocolloids, 166*. https://doi.org/10.1016/j.foodhyd.2025.111387

Hellwig, M. (2020). Analysis of protein oxidation in food and feed products. *Journal of Agricultural and Food Chemistry, 68*(46), 12870–12885. https://doi.org/10.1021/acs.jafc.0c00711

Hishida, M., Kaneko, A., Yamamura, Y., & Saito, K. (2023). Contrasting changes in strongly and weakly bound hydration water of a protein upon denaturation. *The Journal of Physical Chemistry. B, 127*(28), 6296–6305. https://doi.org/10.1021/acs.jpcb.3c02970

Huang, X., Liu, Y., Zou, Y., Liang, X., Peng, Y., McClements, D. J., & Hu, K. (2019). Encapsulation of resveratrol in zein/pectin core-shell nanoparticles: Stability, bioaccessibility, and antioxidant capacity after simulated gastrointestinal digestion. *Food Hydrocolloids, 93*, 261–269. https://doi.org/10.1016/j.foodhyd.2019.02.039

Jain, A., Sharma, G., Kushwah, V., Ghoshal, G., Jain, A., Singh, B., … Katare, O. P. (2018). Beta carotene-loaded zein nanoparticles to improve the biopharmaceutical attributes and to abolish the toxicity of methotrexate: A preclinical study for breast cancer. *Artificial Cells, Nanomedicine, and Biotechnology, 46*(sup1), 402–412. https://doi.org/10.1080/21691401.2018.1428811

Jin, S., Reverdatto, S. V., Ermolenkov, V. V., Shekhtman, A., Jung, Y. M., & Lednev, I. K. (2026). Encapsulation of mRNA in therapeutics like lipid nanoparticles probed by deep-UV resonance Raman spectroscopy. *Analytical Chemistry, 98*(5), 3523–3530. https://doi.org/10.1021/acs.analchem.5c04246

Joye, I. J., Davidov-Pardo, G., Ludescher, R. D., & McClements, D. J. (2015). Fluorescence quenching study of resveratrol binding to zein and gliadin: Towards a more rational approach to resveratrol encapsulation using water-insoluble proteins. *Food Chemistry, 185*, 261–267. https://doi.org/10.1016/j.foodchem.2015.03.128

Kitchen, D. B., Decornez, H., Furr, J. R., & Bajorath, J. (2004). Docking and scoring in virtual screening for drug discovery: Methods and applications. *Nature Reviews. Drug Discovery, 3*(11), 935–949. https://doi.org/10.1038/nrd1549

Knockaert, G., Pulissery, S. K., Lemmens, L., Van Buggenhout, S., Hendrickx, M., & Van Loey, A. (2012). Carrot beta-carotene degradation and isomerization kinetics during thermal processing in the presence of oil. *Journal of Agricultural and Food Chemistry, 60*(41), 10312–10319. https://doi.org/10.1021/jf3025776

Kolašinac, S., Pećinar, I., Danojević, D., Aćić, S., & Stevanović, Z. D. (2021). Raman spectroscopic-based chemometric modeling in assessment of red pepper ripening phases and carotenoids accumulation. *Journal of Raman Spectroscopy, 52*(9), 1598–1605. https://doi.org/10.1002/jrs.6197

Lakowicz, J. R. (2006). Protein fluorescence. In J. R. Lakowicz (Ed.), *Principles of fluorescence spectroscopy* (pp. 529–575). Springer US. https://doi.org/10.1007/978-0-387-46312-4_16.

Lan, T., Dong, Y., Jiang, L., Zhang, Y., & Sui, X. (2024). Analytical approaches for assessing protein structure in protein-rich food: A comprehensive review. *Food Chem X, 22*, Article 101365. https://doi.org/10.1016/j.fochx.2024.101365

Lei, Y., & Lee, Y. (2024). Nanoencapsulation and delivery of bioactive ingredients using zein nanocarriers: Approaches, characterization, applications, and perspectives. *Food Science and Biotechnology, 33*(5), 1037–1057. https://doi.org/10.1007/s10068-023-01489-6

Li, H., Wang, D., Liu, C., Zhu, J., Fan, M., Sun, X., Wang, T., Xu, Y., & Cao, Y. (2019). Fabrication of stable zein nanoparticles coated with soluble soybean polysaccharide for encapsulation of quercetin. *Food Hydrocolloids, 87*, 342–351. https://doi.org/10.1016/j.foodhyd.2018.08.002

Li, R., Huang, L., Zhang, Z., Chen, J., & Tang, H. (2022). Integrated multispectroscopic analysis and molecular docking analyses of the structure-affinity relationship and mechanism of the interaction of flavonoids with zein. *Food Chemistry, 386*, Article 132839. https://doi.org/10.1016/j.foodchem.2022.132839

Liang, L., & Zheng, Q. (2023). Insights into the binding mechanism between alpha-TOH and CYP4F2: A homology modeling, molecular docking, and molecular dynamics simulation study. *Journal of Cellular Biochemistry, 124*(4), 573–585. https://doi.org/10.1002/jcb.30391

Liu, F., Ma, C., McClements, D. J., & Gao, Y. (2017). A comparative study of covalent and non-covalent interactions between zein and polyphenols in ethanol-water solution. *Food Hydrocolloids, 63*, 625–634. https://doi.org/10.1016/j.foodhyd.2016.09.041

Liu, G., Pang, J., Huang, Y., Xie, Q., Guan, G., & Jiang, Y. (2017). Self-assembled nanospheres of folate-decorated zein for the targeted delivery of 10-hydroxycamptothecin. *Industrial & Engineering Chemistry Research, 56*(30), 8517–8527. https://doi.org/10.1021/acs.iecr.7b01632

Liu, W.-L., Zheng, Z.-R., Zhu, R.-B., Liu, Z.-G., Xu, D.-P., Yu, H.-M., … Su, W.-H. (2007). Effect of pressure and solvent on Raman spectra of all-trans-β-carotene. *The Journal of Physical Chemistry A, 111*(40), 10044–10049. https://doi.org/10.1021/jp074048b

Liu, Y., Hou, Z., Yang, J., & Gao, Y. (2015). Effects of antioxidants on the stability of beta-carotene in O/W emulsions stabilized by gum Arabic. *Journal of Food Science and Technology, 52*(6), 3300–3311. https://doi.org/10.1007/s13197-014-1380-0

Lorenz-Fonfria, V. A. (2020). Infrared difference spectroscopy of proteins: From bands to bonds. *Chemical Reviews, 120*(7), 3466–3576. https://doi.org/10.1021/acs.chemrev.9b00449

Lu, Y., Cai, X., Lv, W., Duan, C., Li, X., Ma, F., & Li, D. (2024). Multispectral analysis and molecular docking to predict the mechanism of molecular interactions of curcumin, zein and fucoidan complexes. *Journal of Food Engineering, 369*. https://doi.org/10.1016/j.jfoodeng.2024.111953

Mahalakshmi, L., Leena, M. M., Moses, J. A., & Anandharamakrishnan, C. (2020). Micro- and nano-encapsulation of beta-carotene in zein protein: Size-dependent release and absorption behavior. *Food & Function, 11*(2), 1647–1660. https://doi.org/10.1039/c9fo02088h

Marin, E., Bristol, D. R., Rondinella, A., Lanzutti, A., & Riello, P. (2024). Statistical approaches to Raman imaging: principal component score mapping. *Analytical Methods, 16*(17), 2707–2720. https://doi.org/10.1039/d4ay00171k

Martiel, I., Sagalowicz, L., & Mezzenga, R. (2014). Phospholipid-based nonlamellar mesophases for delivery systems: Bridging the gap between empirical and rational design. *Advances in Colloid and Interface Science, 209*, 127–143. https://doi.org/10.1016/j.cis.2014.03.005

Mastronarde, D. N. (2005). Automated electron microscope tomography using robust prediction of specimen movements. *Journal of Structural Biology, 152*(1), 36–51. https://doi.org/10.1016/j.jsb.2005.07.007

Medina-Gutiérrez, C., Frausto-Reyes, C., Medina-Valtierra, J., Jaimes-Reátegui, R., García-López, H., & Molina-Contreras, J. R. (2006). Study of temperature effect in β-carotene of carrot by Raman spectroscopy. In *Fifth Symposium Optics in Industry*. Santiago De Queretaro, Mexico.

Meinhardt-Wollweber, M., Suhr, C., Kniggendorf, A.-K., & Roth, B. (2018). Absorption and resonance Raman characteristics of β-carotene in water-ethanol mixtures, emulsion and hydrogel. *AIP Advances, 8*(5). https://doi.org/10.1063/1.5025788

Mohammadian, M., Waly, M. I., Moghadam, M., Emam-Djomeh, Z., Salami, M., & Moosavi-Movahedi, A. A. (2020). Nanostructured food proteins as efficient systems for the encapsulation of bioactive compounds. *Food Science and Human Wellness, 9*(3), 199–213. https://doi.org/10.1016/j.fshw.2020.04.009

Musa, H. H., Ahmed, A. A., & Musa, T. H. (2018). Chemistry, biological, and pharmacological properties of gum Arabic. In *Sweeteners* (pp. 1–18). https://doi.org/10.1007/978-3-319-54528-8_11-1

Nair, M. S. (2017). Spectroscopic studies on the interaction of serum albumins with plant derived natural molecules. *Applied Spectroscopy Reviews, 53*(8), 636–666. https://doi.org/10.1080/05704928.2017.1402184

Norbert, S. (2007). *X-Ray scattering of soft matter*. Springer.

Novikov, V. S., Kuzmin, V. V., Kuznetsov, S. M., Darvin, M. E., Lademann, J., Sagitova, E. A., … Nikolaeva, G. Y. (2021). DFT study of Raman spectra of polyenes and ss-carotene: Dependence on length of polyene chain and isomer type. *Spectrochimica Acta. Part A, Molecular and Biomolecular Spectroscopy, 255*, Article 119668. https://doi.org/10.1016/j.saa.2021.119668

Orlando, A., Franceschini, F., Muscas, C., Pidkova, S., Bartoli, M., Rovere, M., & Tagliaferro, A. (2021). A comprehensive review on Raman spectroscopy applications. *Chemosensors, 9*(9). https://doi.org/10.3390/chemosensors9090262

Pan, K., Luo, Y., Gan, Y., Baek, S. J., & Zhong, Q. (2014). pH-driven encapsulation of curcumin in self-assembled casein nanoparticles for enhanced dispersibility and bioactivity. *Soft Matter, 10*(35), 6820–6830. https://doi.org/10.1039/c4sm00239c

Pan, L., Zhang, P., Daengngam, C., Peng, S., & Chongcheawchamnan, M. (2021). A review of artificial intelligence methods combined with Raman spectroscopy to identify the composition of substances. *Journal of Raman Spectroscopy, 53*(1), 6–19. https://doi.org/10.1002/jrs.6225

Pascoli, M., de Lima, R., & Fraceto, L. F. (2018). Zein nanoparticles and strategies to improve colloidal stability: A mini-review. *Frontiers in Chemistry, 6*, 6. https://doi.org/10.3389/fchem.2018.00006

Peters, J., Kornmueller, K., Dannaoui, R., Syla, E., & Pastore, A. (2024). Direct detection of bound water in hydrated powders of lysozyme by differential scanning calorimetry. *ACS Physical Chemistry Au, 4*(6), 593–597. https://doi.org/10.1021/acsphyschemau.4c00029

Portarena, S., Anselmi, C., Leonardi, L., Proietti, S., Bizzarri, A. R., Brugnoli, E., & Baldacchini, C. (2023). Lutein/beta-carotene ratio in extra virgin olive oil: An easy and rapid quantification method by Raman spectroscopy. *Food Chemistry, 404*(Pt B), Article 134748. https://doi.org/10.1016/j.foodchem.2022.134748

Poudyal, M., Patel, K., Gadhe, L., Sawner, A. S., Kadu, P., Datta, D., … Maji, S. K. (2023). Intermolecular interactions underlie protein/peptide phase separation irrespective of sequence and structure at crowded milieu. *Nature Communications, 14*(1), 6199. https://doi.org/10.1038/s41467-023-41864-9

Qiang, S., Zhou, J., Yang, T., Wang, J., Chen, Y., Chen, G., & Li, S. (2024). Structure, stability and in vitro digestion of a novel zein-based oil gel delivery system loaded β-carotene. *Journal of Food Engineering, 366*. https://doi.org/10.1016/j.jfoodeng.2023.111848

Qiu, C., Zhang, Z., Li, X., Sang, S., McClements, D. J., Chen, L., … Jin, Z. (2023). Co-encapsulation of curcumin and quercetin with zein/HP-beta-CD conjugates to enhance environmental resistance and antioxidant activity. *npj Science of Food, 7*(1), 29. https://doi.org/10.1038/s41538-023-00186-2

Ramos, R., Bernard, J., Ganachaud, F., & Miserez, A. (2022). Protein-based encapsulation strategies: Toward micro- and nanoscale carriers with increased functionality. *Small Science, 2*(3). https://doi.org/10.1002/smsc.202100095

Ren, P., Zhou, R.-G., & Li, Y. (2025). A self-supervised learning method for Raman spectroscopy based on masked autoencoders. *Expert Systems with Applications, 292*. https://doi.org/10.1016/j.eswa.2025.128576

Sabet, S., Rashidinejad, A., Melton, L. D., Zujovic, Z., Akbarinejad, A., Nieuwoudt, M., … McGillivray, D. J. (2021). The interactions between the two negatively charged

polysaccharides: Gum Arabic and alginate. *Food Hydrocolloids, 112*. https://doi.org/10.1016/j.foodhyd.2020.106343
Sadat, A., Corradini, M. G., & Joye, I. J. (2022). Vibrational and fluorescence spectroscopy to study gluten and zein interactions in complex dough systems. *Current Research in Food Science, 5*, 479–490. https://doi.org/10.1016/j.crfs.2022.02.009
Saito, S., & Tasumi, M. (1983). Normal-coordinate analysis of β-carotene isomers and assignments of the Raman and infrared bands. *Journal of Raman Spectroscopy, 14*(5), 310–321. https://doi.org/10.1002/jrs.1250140504
Schindelin, J., Arganda-Carreras, I., Frise, E., Kaynig, V., Longair, M., Pietzsch, T., … Cardona, A. (2012). Fiji: An open-source platform for biological-image analysis. *Nature Methods, 9*(7), 676–682. https://doi.org/10.1038/nmeth.2019
Sethuraman, S., & Rajendran, K. (2018). Multicharacteristic behavior of tyrosine present in the microdomains of the macromolecule gum arabic at various pH conditions. *ACS Omega, 3*(12), 17602–17609. https://doi.org/10.1021/acsomega.8b02928
Sethuraman, S., & Rajendran, K. (2019). Is gum arabic a good emulsifier due to CH...Pi interactions? How urea effectively destabilizes the hydrophobic CH...pi interactions in the proteins of gum arabic than amides and GuHCl? *ACS Omega, 4*(15), 16418–16428. https://doi.org/10.1021/acsomega.9b01980
Shibasaki-Kitakawa, N., Murakami, M., Kubo, M., & Yonemoto, T. (2011). A kinetic model describing antioxidation and prooxidation of β-carotene in the presence of α-tocopherol and ascorbic acid. *Journal of the American Oil Chemists' Society, 89*(5), 815–824. https://doi.org/10.1007/s11746-011-1980-z
Shukla, R., & Cheryan, M. (2001). Zein: The industrial protein from corn. *Industrial Crops and Products, 13*(3), 171–192. https://doi.org/10.1016/S0926-6690(00)00064-9
Sousa, F., Cruz, A., Fonte, P., Pinto, I. M., Neves-Petersen, M. T., & Sarmento, B. (2017). A new paradigm for antiangiogenic therapy through controlled release of bevacizumab from PLGA nanoparticles. *Scientific Reports, 7*(1), 3736. https://doi.org/10.1038/s41598-017-03959-4
Sun, C., Dai, L., & Gao, Y. (2016). Binary complex based on zein and propylene glycol alginate for delivery of quercetagetin. *Biomacromolecules, 17*(12), 3973–3985. https://doi.org/10.1021/acs.biomac.6b01362
Sun, D.-W., Pu, H., & Yu, J. (2024). Applications of hyperspectral imaging technology in the food industry. *Nature Reviews Electrical Engineering, 1*(4), 251–263. https://doi.org/10.1038/s44287-024-00033-w
Tadele, D. T., Islam, M. S., & Mekonnen, T. H. (2025). Zein-based nanoparticles and nanofibers: Co-encapsulation, characterization, and application in food and biomedicine. *Trends in Food Science & Technology, 155*. https://doi.org/10.1016/j.tifs.2024.104809
Tadele, D. T., & Mekonnen, T. H. (2024). Co-encapsulation of quercetin and α-tocopherol bioactives in zein nanoparticles: Synergistic interactions, stability, and controlled release. *ACS Applied Polymer Materials, 6*(7), 3767–3777. https://doi.org/10.1021/acsapm.3c03000
Takma, D. K., Bozkurt, S., Koç, M., Korel, F., & Nadeem, H.Ş. (2023). Characterization and encapsulation efficiency of zein nanoparticles loaded with chestnut fruit shell, cedar and sweetgum bark extracts. *Food Hydrocolloids for Health, 4*. https://doi.org/10.1016/j.fhfh.2023.100151
Tan, H., Zhou, H., Guo, T., Zhou, Y., Zhang, Y., Yuan, R., & Ma, L. (2024). pH-induced interaction mechanism of zearalenone with zein: Binding characteristics, conformational structure and intermolecular forces. *Food Chemistry, 444*, Article 138595. https://doi.org/10.1016/j.foodchem.2024.138595
Tarhini, M., Greige-Gerges, H., & Elaissari, A. (2017). Protein-based nanoparticles: From preparation to encapsulation of active molecules. *International Journal of Pharmaceutics, 522*(1–2), 172–197. https://doi.org/10.1016/j.ijpharm.2017.01.067
Team, R. C. (2025). *R: A language and environment for statistical computing*. (Version 4.5.0) R Foundation for Statistical Computing. https://www.R-project.org/.
Tiwari, P., Ali, R., Ishrat, R., & Arfin, N. (2021). Study of interaction between zein and curcumin using spectroscopic and in silico techniques. *Journal of Molecular Structure, 1230*. https://doi.org/10.1016/j.molstruc.2020.129637
Trott, O., & Olson, A. J. (2010). AutoDock Vina: Improving the speed and accuracy of docking with a new scoring function, efficient optimization, and multithreading. *Journal of Computational Chemistry, 31*(2), 455–461. https://doi.org/10.1002/jcc.21334
Wang, M., Fu, Y., Chen, G., Shi, Y., Li, X., Zhang, H., & Shen, Y. (2018). Fabrication and characterization of carboxymethyl chitosan and tea polyphenols coating on zein nanoparticles to encapsulate β-carotene by anti-solvent precipitation method. *Food Hydrocolloids, 77*, 577–587. https://doi.org/10.1016/j.foodhyd.2017.10.036
Wang, N., Fan, H., Wang, J., Wang, H., & Liu, T. (2024). Fabrication and characterization of curcumin-loaded composite nanoparticles based on high-hydrostatic-pressure-treated zein and pectin: Interaction mechanism, stability, and bioaccessibility. *Food Chemistry, 446*, Article 138286. https://doi.org/10.1016/j.foodchem.2023.138286
Wang, X., & Fan, M. (2019). Interaction behaviors and structural characteristics of zein/NaTC nanoparticles. *RSC Advances, 9*(10), 5748–5755. https://doi.org/10.1039/c9ra00005d
Wang, X., Zhang, X., Hong, H., Guan, C., & Zhao, C. (2021). Non-destructive quantitative analysis of carotene content in carrots using Raman spectroscopy. *European Food Research and Technology, 247*(9), 2299–2307. https://doi.org/10.1007/s00217-021-03788-w
Wei, Y., Wang, C., Liu, X., Mackie, A., Zhang, M., Dai, L., Liu, J., Mao, L., Yuan, F., & Gao, Y. (2022). Co-encapsulation of curcumin and β-carotene in Pickering emulsions stabilized by complex nanoparticles: Effects of microfluidization and thermal treatment. *Food Hydrocolloids, 122*. https://doi.org/10.1016/j.foodhyd.2021.107064
Wu, X., Zhao, X., Deng, Z., Liang, X., & Fang, S. (2021). Investigation of interactions between zein and natamycin by fluorescence spectroscopy and molecular dynamics simulation. *Journal of Molecular Liquids, 327*. https://doi.org/10.1016/j.molliq.2020.114873
Xu, Z., Zhang, X., Wu, X., Ma, D., Huang, Y., Zhao, Q., … Li, Y. (2024). Co-delivery of vitamin C and beta-carotene in W/O/W emulsions stabilized by modified aggregated insoluble soybean protein hydrolysate-xanthan gum complexes. *International Journal of Biological Macromolecules, 261*(Pt 2), Article 129855. https://doi.org/10.1016/j.ijbiomac.2024.129855
Yakoubi, S. (2024). Enhancing plant-based cheese formulation through molecular docking and dynamic simulation of tocopherol and retinol complexes with zein, soy and almond proteins via SVM-machine learning integration. *Food Chemistry, 452*, Article 139520. https://doi.org/10.1016/j.foodchem.2024.139520
Yang, J., Palla, M., Bosco, F. G., Rindzevicius, T., Alstrøm, T. S., Schmidt, M. S., … Lin, Q. (2013). Surface-enhanced Raman spectroscopy based quantitative bioassay on aptamer-functionalized nanopillars using large-area Raman mapping. *ACS Nano, 7*(6), 5350–5359. https://doi.org/10.1021/nn401199k
Yu, X., Afreen, S., Kong, Q., & Wang, J. (2020). Study on self-assembled morphology and structure regulation of alpha-zein in ethanol-water mixtures. *Langmuir, 36*(40), 11975–11984. https://doi.org/10.1021/acs.langmuir.0c02143
Yu, Y., & Liang, G. (2022). Interaction mechanism of phenolic acids and zein: A spectrofluorometric and molecular dynamics investigation. *Journal of Molecular Liquids, 348*. https://doi.org/10.1016/j.molliq.2021.118032
Yuan, Y., Ma, M., Wang, D., & Xu, Y. (2023). A review of factors affecting the stability of zein-based nanoparticles loaded with bioactive compounds: From construction to application. *Critical Reviews in Food Science and Nutrition, 63*(25), 7529–7545. https://doi.org/10.1080/10408398.2022.2047881
Yue, X. J., Xu, P. W., Luo, X. C., & Zhao, B. (2024). Multi-spectroscopies and molecular docking insights into the interaction mechanism and antioxidant activity of isoquercetin and zein nanoparticles. *International Journal of Biological Macromolecules, 263*(Pt 1), Article 130412. https://doi.org/10.1016/j.ijbiomac.2024.130412
Zhang, F., Khan, M. A., Cheng, H., & Liang, L. (2019). Co-encapsulation of α-tocopherol and resveratrol within zein nanoparticles: Impact on antioxidant activity and stability. *Journal of Food Engineering, 247*, 9–18. https://doi.org/10.1016/j.jfoodeng.2018.11.021
Zhang, J., Qi, H., Wang, M., Wei, Y., & Liang, H. (2023). Enzymatically hydrolyzed sodium caseinate nanoparticles efficiently enhancing the solubility, stability, and antioxidant and anti-biofilm activities of hydrophobic Tanshinone IIA. *Journal of Materials Chemistry B, 11*(11), 2440–2454. https://doi.org/10.1039/d2tb02263j
Zhang, X., Liu, Y., Zheng, B., Zang, J., Lv, C., Zhang, T., … Zhao, G. (2021). Protein interface redesign facilitates the transformation of nanocage building blocks to 1D and 2D nanomaterials. *Nature Communications, 12*(1), 4849. https://doi.org/10.1038/s41467-021-25199-x
Zhang, Y., Zhao, W., Xing, Z., Zhu, B., Hou, R., Zhang, J., … Li, Z. (2022). Study on the binding behavior and functional properties of soybean protein isolate and beta-carotene. *Frontiers in Nutrition, 9*, Article 984490. https://doi.org/10.3389/fnut.2022.984490
Zhang, Z., Li, R., Tang, H., & Li, J.-X. (2023). Interactions and characterization of Zein-BSA nanoparticles: Multi-spectral analysis and molecular simulations. *Journal of Molecular Liquids, 391*. https://doi.org/10.1016/j.molliq.2023.123293
Zhao, S., Deng, Y., Yan, T., Yang, X., Xu, W., Liu, D., & Wang, W. (2022). Explore the interaction between ellagic acid and zein using multi-spectroscopy analysis and molecular docking. *Foods, 11*(18). https://doi.org/10.3390/foods11182764
Zhou, Y., Tang, X., Zhang, D., & Lee, H. J. (2025). Machine learning empowered coherent Raman imaging and analysis for biomedical applications. *Communications Engineering, 4*(1), 8. https://doi.org/10.1038/s44172-025-00345-1
Zhu, J., Sun, W., Zhang, W., Hong, N., Liao, Y., Yao, Y., Cai, L., Xiong, C., & Yao, L. (2024). A joint experimental and theoretical investigation of the binding mechanism between zein and folic acid in an ethanol–water solution. *International Journal of Food Properties, 27*(1), 729–749. https://doi.org/10.1080/10942912.2024.2357609
Zhu, J., Yao, Y., Liao, Y., Cai, L., Zhang, W., Hong, N., … Yao, L. (2024). The interaction mechanism between zein and folic acid in alkaline aqueous solutions: An experimental and molecular simulation study. *Food Quality and Safety, 8*. https://doi.org/10.1093/fqsafe/fyad064
Zimath, P., Pinto, S., Dias, S., Rafacho, A., & Sarmento, B. (2023). Zein nanoparticles as oral carrier for mometasone furoate delivery. *Drug Delivery and Translational Research, 13*(11), 2948–2959. https://doi.org/10.1007/s13346-023-01367-y